Int. J. Electrochem. Sci., 9 **(2014)** 7021 - 7037

International Journal of
ELECTROCHEMICAL
SCIENCE
www.electrochemsci.org

Structure and Properties of Electro Co-Deposited Ni-Fe/ZrO_2 Nanocomposites from Ethylene Glycol Bath

Alok Kumar Chaudhari and V. B. Singh[*]

Department of Chemistry, Banaras Hindu University, Varanasi 221005, India
[*]E-mail: vijaybs@bhu.ac.in

Received: 19 July 2014 / *Accepted:* 29 August 2014 / *Published:* 29 September 2014

Ni-Fe/ZrO_2 nanocomposite coatings were prepared by electrodeposition under direct current condition from nickel sulfamate and ferrous sulphate bath with ZrO_2 nanopowder using ethylene glycol as a solvent. Plating parameters like current density, concentration of ZrO_2 particles and electrolytes, temperature and agitation were optimized in terms of particle incorporation, microhardness and brightness of the deposits. Morphology, composition, micro and crystallographic structures of the coatings were investigated by SEM, EDAX, XRD and TEM. The iron content in the deposit varies from 38.2% to 19.1% showing fcc lattice by the Ni-Fe alloy matrix. Due to incorporation of ZrO_2 particles in Ni-Fe matrix average crystallite size of the deposit reduces to ≈11 nm. The effect of current density and annealing temperature on microstructure, texture and microhardness was studied. With increasing current density from 1.0 to 5.0 A/dm^2 there is shifting of preferred orientation from (111) to (220) crystallographic plane.

Keywords: Electrodeposition; nanocomposites; Ni-Fe/ZrO_2 coating; XRD; TEM; Microhardness.

1. INTRODUCTION

Electrodeposition technique is a “one step- bottom up” approach of codepositing fine particles of metallic, non-metallic compounds or polymers for producing metal matrix composites. Metal matrix composites have improved material properties such as wear resistance, high temperature corrosion protection, oxidation resistance, enhanced super-plasticity at relatively low temperatures, self lubrication etc. Such a composite coating consists of a metal or alloy matrix reinforced with different second phase particles of micro and nano size like oxides, carbides nitrides etc. e.g. TiC[1], Al_2O_3[2], ZrO_2[3,4,5] , $SrSO_4$[6], SiC[7,8,9], BN[10]. The improvement of properties of the metallic composites is dependent mainly on the size and percentage of the particles co-deposited as well as on the distribution of the particles in the matrix [8,11]. With the emergence of reinforcing powders with ever

decreasing particle size over the last decade, electrodeposition techniques have provided an alternative route to obtain a variety of new nanomaterials (nanocomposites) with improved and well controlled properties. The nanocomposite coatings produced, usually exhibit enhanced properties as compared to monolithic metal coating as well as micro- composite coatings[12] such as mechanical properties , tribological properties[8], enhanced electrical resistance, micro- electro-mechanical systems (MEMS)[10,13]. With the increasing availability of nanoparticles, the interest for electrolytic and electroless composite coatings containing nanoparticles is growing. The major challenges with the co-deposition of nanoparticles are the achievement of a high level of co-deposition, and avoiding agglomeration of particles suspended in the electrolytes.

In metal matrix ceramic composite coatings, ceramic particles play a major role for improving the properties of composites/nanocomposites. ZrO_2being an inert ceramic has many superior properties such as excellent thermal, chemical and mechanical stability as well as unique optical and dielectric properties. ZrO_2 has been widely used in corrosion resistant coatings due to its lower corrosion current density probably due to changing of microstructure from coarse grained to fine grained structure. It has very high melting temperature (M.P.>2700^oC), high volume resistivity (> 10^{10} Ohm.cm) and thus has good electrical insulating properties. After insulating ZrO_2 in Ni matrix an increase in the microhardness has been reported [3,4,12,14,15]. Due to the above advantages, ZrO_2 is used as reinforcing agent with many metal/ alloy matrices such as Ni-Co-ZrO_2 [4]. Ag-ZrO_2[16], Co-ZrO_2[17], Cr-ZrO_2[18], Ni-W-P-ZrO_2[19], Ni-ZrO_2[20,21], Zn-ZrO_2[22], PbO_2-ZrO_2[23], Ni-Fe-ZrO_2[24].

Nickel is an engineering material which has been widely used as metal matrix [3,5,6,8,25]. Zirconia and nickel have a good compatibility because of their similar thermal expansion coefficient and elastic modulus[5]. The high cost of nickel motivates to substitute nickel by less expensive metal with improved properties. Therefore much attention has been directed to the studies of iron nickel alloys and their composites/nanocomposites due to their interesting mechanical and magnetic properties[26-29]. Due to soft magnetic properties, higher microhardness, good ductility, and other promising practical applications, Ni-Fe (20 wt% Fe permalloy) is highly demanding material, which is used in transformer lamination, magnetic recording head sensors, watch parts, floppy disc drive and car speedometer etc.

Electrodeposition of Ni-Fe alloy is classified as anomalous co-deposition because of the preferential deposition of the less noble metal ie. Fe[10,30-33]. Ni-Fe alloys and their composites have been electrodeposited and their properties have been extensively investigated in aqueous bath[17,30,31,33,34]. It was found that discharge of hydrogen takes place during plating using aqueous media which can significantly influence the deposition process and crystallographic structure[35]. The discharge of H^+ ions and evolution of hydrogen during electrodeposition of metal coating were major disadvantages of aqueous bath. Thus we have to search a suitable solvent which have either no active hydrogen or hydrogen is more strongly bounded than water. Several researches in the past few years included a study of the electrodeposition of metals from solutions of their salts in organic solvents like N-methyl formamide[9,36], N,N-dimethyl formamide[10,36] etc. in order to escape the otherwise consequences of hydrogen evolved and occluded in metal during electrodeposition from aqueous solution. Ethylene glycol is a amphoteric neutral solvent having a high donor number (20), higher density (1.1132 g/cm^3) and viscosity (16.1 cp) than water and good complexing nature towards metal

ions. Zirconia particles forms better suspension due to wetability in this solvent. Thus ethylene glycol possesses the properties of an excellent solvent for electrodeposition of metal and alloys and because of this it has been used by some other workers[37,38] for this purpose in the past.

Ferrous sulphate is most commonly used for preparing the iron alloy plating baths because the deposition of the iron from the ferric ion occurs with a low cathode current efficiency. Nickel sulfamate plating baths are odorless and have no more noticeable effect upon producing skin irritations. The major advantages of sulfamate bath include – (I) yielding in stress free deposits, (II) high current density operations at low temperatures, (III) low sensitivity to impurities, (IV) deposits of high chemical purity, (V) improvement of fatigue strength, (VI) excellent grain structure and ductility. (VII) grains are fine, deposits are very smooth and much brighter. Therefore it becomes very interesting to study the electrodeposition of metal matrix nanocomposites from ethylene glycol (organic) bath which may provide coatings with improved properties than the conventional aqueous bath.

The present study is aimed at incorporating ZrO_2 particles to a maximum extent in the Ni-Fe alloy matrix by electrodeposition method on the copper substrate in an organic solvent (ethylene glycol) by varying different deposition parameters e.g. concentration of electrolyte and particle, current density, temperature, agitation etc. and to study it's influence on the content as well as distribution of ZrO_2 particles in the alloy matrix, mechanical properties and microstructure.

2. EXPERIMENTAL

Table 1. Bath composition and plating conditions for the electrodeposition of Ni-Fe/ZrO_2 nanocomposites in ethylene glycol bath.

Parameter	Value
Nickel sulfamate, g/l	100.0
Ferrous sulphate, g/l	4.0
Boric Acid, g/l	30.0
ZrO_2 nanopowder, g/l	5.0
Duration of electrolysis, minute	30-90
Temperature, °C	34°C ± 0.5
Current density, A/dm^2	1.0 – 5.0
Agitation, rpm	700 ± 5

Ni-Fe/ZrO_2 nanocomposites were electrodeposited on copper substrate from an additive free bath consisting of Nickel sulfamate tetrahydrate (Fluka), Ferrous sulphate heptahydrate (Fisher scientific India), Boric acid (Qualigens fine chemicals , India), Zirconium dioxide nanopowder <100 nm (Sigma Aldrich) in Ethylene glycol (Qualigens fine chemicals, India). All chemicals were of analytical grade and used without further purification. The electrolytic bath solution containing 100 g/l of nickel sulfamate tetrahydrate, 4 g/l of ferrous sulphate heptahydrate, 30 g/l of boric acid produces

coatings of permalloy composition and in order to get composite of the permalloy, 5 g/l ZrO_2 particles were dispersed in the same electrolytic bath. The conditions for composite deposition are given in table – 1.

Highly polished[1,9] copper plates of 2 cm X 1 cm X 0.1 cm dimension were placed between two parallel rectangular pure nickel anodes. Homogeneous suspension of ZrO_2 particles in the electrolytic solution is obtained by blending ZrO_2 nanopowder and other electrolytes with a small quantity of solvent (ethylene glycol) to get slurry. The electrolytic solution is prepared by transferring the slurry to appropriate volume of ethylene glycol and mechanically stirred for four hours. The suspension of ZrO_2 particles was maintained in the bath during electrolysis by continuous agitation with the help of a small panel fan stirred at the rate of 200-1500 rpm, which was fitted in electrolytic cell assembly equipped with digital speedometer. The electrolysis was carried out at current density 1.0-5.0 A/dm^2 for varying duration (30-90 min) depending on the current density applied. To maintain a uniform temperature (34°C) inside the cell, the electrolysis cell was placed in a thermostat (HAAKE DC 30, India). The extent of ZrO_2 particles incorporation in the Ni-Fe alloy matrix, mechanical and thermal properties of the deposits were studied at different current density. Conditions were optimized for Ni-Fe/ZrO_2 nanocomposites by varying one parameter at a time while others were kept to a fixed value.

After the deposition, the cathode was ultrasonically cleaned for 10 minutes (Cody, CD-2800 Japan). The orientation of the electrodeposited Ni-Fe/ZrO_2 nanocomposites were examined by X-ray diffractometer (Rigaku mini flex II) using Cu Kα radiation (λ=1.541836 Å) within 20-90° 2θ Bragg's angle range. Crystallite size and strain of the nanocomposite was calculated by the single line profile analysis of the most intense peak in the X-ray diffractogram. The apparent crystallite size D and strain η can be related to integral breadth of the line β and corresponding Bragg's angle θ.

$D = \lambda/\beta \cos\theta$ ….[39] and

$\eta = \beta/4\tan\theta$ .....[40]

The relative texture coefficient {$RTC_{(hkl)}$} was calculated as follows:

$RTC_{(hkl)} = I_{(hkl)}/I^{o}_{(hkl)} \{\Sigma(I_{(hkl)}/I^{o}_{(hkl)}\}^{-1} X\ 100$

Where $I_{(hkl)}$ are the diffraction intensities of the (hkl) lines measured in XRD pattern of the deposits and $I^{o}_{(hkl)}$ are the corresponding intensities of a standard Ni powder sample randomly oriented.

The electrochemical polarization studies were carried out using a Wenking POS 73 potentiostate. Prior to polarization measurements, the steady-state open circuit potential of the electrode was recorded over 30 minutes to allow dynamic stabilization between the working electrode and electrolyte. The potentials were applied for 2 minutes in order to obtain a stable value and increased by 20 mv each time cathodically starting from OCP. The electrolytic cell was three necked round bottom flask. The three electrodes , copper (cathode), platinum (anode) and saturated calomel electrode as the reference electrode are fitted with round glass joints and can be fixed at certain distance. The cell was placed in an air thermostat chamber. All the cathodic polarization measurements were performed at 34±0.5°C and repeated at least three times to verify the reproducibility of the results.

Scanning electron microscope (SEM, Philips X L20) equipped with energy dispersive X-ray analyzer (EDAX, JEOL 840 A) was used to study the morphology and composition of the

nanocomposites. All the chemical composition values of the deposits are quoted in weight percent (wt%), which is the average of the at least five measurements. The chemical composition of the deposits was also confirmed by chemical analysis. The wt% of Iron content was determined using sulphosalicylic acid[41], which was in good agreement with the results obtained from EDAX. The microstructure and crystallographic structure of the Ni-Fe/ZrO_2 nanocomposite coatings were also examined by TEM (TECNAI G2).

After vaccum sealing in a quartz glass tube, the electrodeposited nanocomposite was annealed for one hour at temperature 800°C and then allowed to cool slowly down to the room temperature. Differential scanning calorimetry (DSC) measurement of the deposits was performed in the temperature range 30 to 660°C under nitrogen atmosphere with heating rate 3°C/minute on DSC 822^e Mettler Toledo equipment.

Microhardness measurements (HV in kilogram force mm^{-2}) of the deposits was performed on surface by microhardness indentation method (Shimadzu, Japan). The microhardness was calculated by the relationship:

$HV = 1854.4\ F/d^2$

Where, HV is expressed in kgf/mm^2, F is force applied in grams and d is the diagonal of the indentation in micrometers. A load of 10 gf for 5 seconds has been applied on the indenter and the corresponding final values were the statistical average of 10 measurements to avoid any substrate effect[42].

3. RESULT AND DISCUSSION

In the present investigation usually smooth, bright and adherent composite coatings were obtained. Stirring rate and bath temperature were optimized for Ni-Fe alloy and Ni-Fe/ZrO_2 nanocomposite, qualitatively, depending on adherence, brightness and smoothness of the deposits observed under optical microscope. It has been found that stirring rate of 700 rpm and 34±0.5°C bath temperature were most suitable for better suspension and desirable quality of deposits.

3.1. Polarization study

The cathodic polarization curves for Ni-ZrO_2, Fe-ZrO_2, and Ni-Fe/ZrO_2 nanocomposites from ethylene glycol bath are illustrated in figure 1. Two distinct regions in the curves are recognized. Firstly the current density does not increase noticeably due to sucessive increase in the cathodic potential and secondly when a certain potential is approached (>640 mv) these curves reveal a rapid increase in the current density. A sharp increase in the current at higher potential indicates the metal deposition to commence with a measurable rate but the deposition is associated with a higher polarization. It can be observed from the cathodic polarization curves that, the curve for Ni-ZrO_2 lies at

less negative potential than that of Fe-ZrO_2 and it indicates the nobler deposition potential of nickel composite than that of iron composite. The polarization curve of the alloy nanocomposite lies between the two parent metal nanocomposites, so it could be expected that nickel should be preferentially deposited and will have more percentage in deposit. However, iron which is less noble metal, deposited preferentially and anomalous co-deposition is observed. It seems reasonable to associate the deposition at higher over potentials in ethylene glycol because of the higher donor number (20) and good complexing tendency to form stable complexes with nickel and iron metal ions[43,44]. Ethylene glycol is a weak field ligand and forms octahedral complexes with both nickel [Ni(Glycol)2sulfamate] and iron [$FeSO_4(Glycol)_3$] metal ions. It is reported that ferrous glycol complexes are less stable than the nickel glycol complexes thus nickel deposition rate is inhibited in the presence of ferrous ion and resulting in anomalous deposition of the alloy-composite [45].

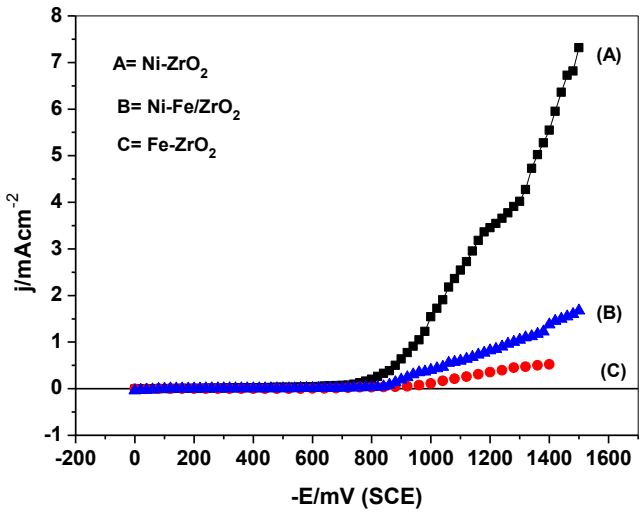

Figure 1. Polarization curves for Fe, Ni and Ni-Fe alloy deposition in ethylene glycol bath in the presence of ZrO_2 particles. (Conditions of the deposition: Nickel sulfamate 100 g/l, ferrous sulphate 4.0 g/l, boric acid 30 g/l, ZrO_2 particle 5.0 g/l, stirring rate 700 rpm, and temperature 34±0.5°C).

3.2 Effect of current density on Ni-Fe alloy and Ni-Fe/ZrO_2 nanocomposite electrodeposition

In electrodeposition process current density is the most important parameter.

Effect of variation in the current density was studied between 1.0 to 5.0 A/dm^2 and good quality deposits were obtained at current density 2.5 to 3.0 A/dm^2. Mirror bright, adherent, uniform, smooth and fine grained deposits were obtained at current density 2.5 A/dm^2 but with further increase in the current density the quality of the deposits gradually deteriorated. Blackish, dull, deposits with peeling on borders and corners were obtained above current density 5.0 A/dm^2. Weight percent of the iron in the deposit decreases from 38.2% to 19.1% with increasing current density from1.0 to 5.0 A/dm^2 (Figure 2). At higher current densities ie. 3.0 to 5.0 A/dm^2 the Fe content of the deposit observes small change (24.0-19.1 weight%) which is close to the composition of permalloy.

The marginal change in the composition of the alloy appears due to diffusion controlled deposition. Figure:3 shows the influence of current density on ZrO_2 particle incorporation in the coating. The particle content in the nanocomposite increased sharply up to current density 2.0 A/dm^2

and thereafter sharply decreased up to current density 4.0 A/dm^2 followed by gradual decrease. The ZrO_2 particles are incorporated along with depositing metal thus rate of particle incorporation is governed by the rate of metal deposition and accessibility of the particles on the cathode surface. It can be argued that in the lower current density region more particles are incorporated with increasing current density because the requirement of particles with increasing metal deposition rate was catered by the mechanical agitation. However, at higher current densities an enhanced deposition of metal occurs and particle incorporation becomes diffusion controlled due to less availability of ZrO_2 particles in respect to higher metal deposition rate.

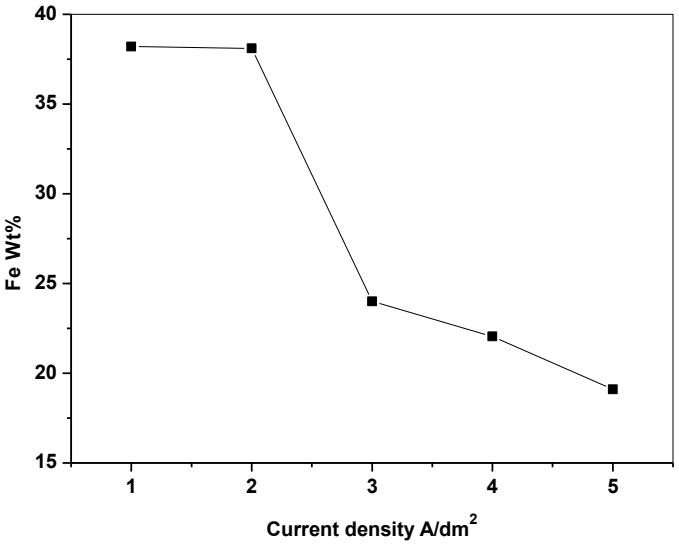

Figure 2. Variation of iron content in the nanocomposite with current density. (Conditions of the deposition: Nickel sulfamate 100 g/l, ferrous sulphate 4.0 g/l, boric acid 30 g/l, ZrO_2 particle 5.0 g/l, stirring rate 700 rpm, and temperature 34±0.5°C).

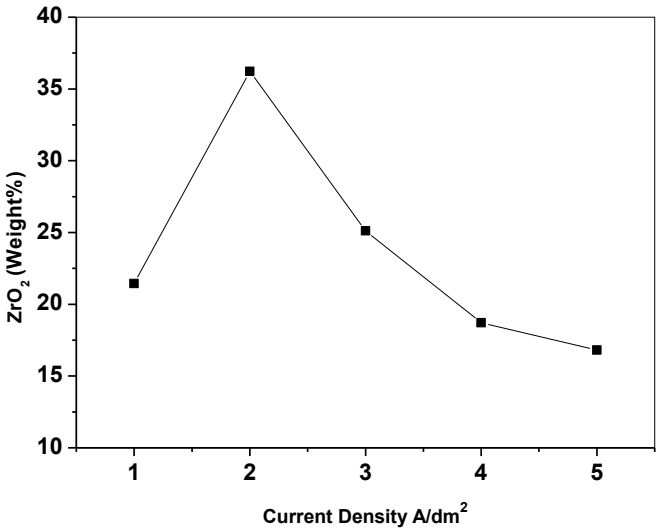

Figure 3. Effect of current density on weight% incorporation ZrO_2 in the deposit. (Conditions of the deposition: Nickel sulfamate 100 g/l, ferrous sulphate 4.0 g/l, boric acid 30 g/l, ZrO_2 particle 5.0 g/l, stirring rate 700 rpm, temperature 34±0.5°C).

Thus at higher current density to a higher value the particle incorporation in the deposit is observed decrease. Similar results have been reported earlier by other investigators also[1,9,46,47].

3.3 Morphology of the Ni-Fe/ZrO_2 nanocomposites: SEM study

The surface morphology of the deposits was preliminary examined by optical microscope and then by Scanning electron microscope (SEM). Smooth surface with white spots is seen in SEM micrographs (figure 4: a, b, c). These images show that, the deposits have very fine granular structure with uniform grains, which is probably because of the grain refinement of the alloy matrix by ZrO_2 particles due to production of larger number of heterogeneous nucleation sites for Ni-Fe matrix on the surface of ZrO_2 particles in various directions affecting their growth and thus having a very fine grained granular structure[20].

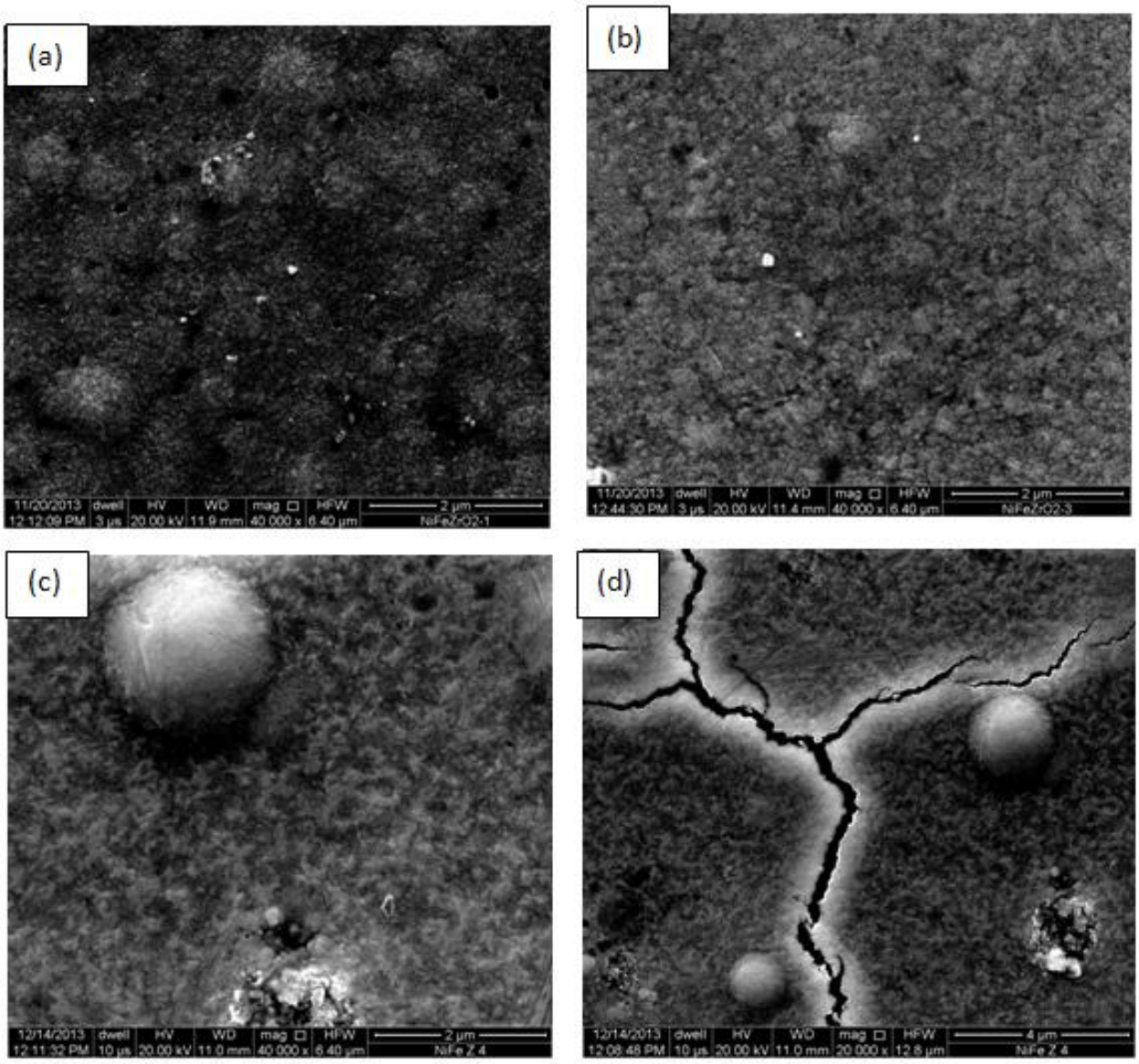

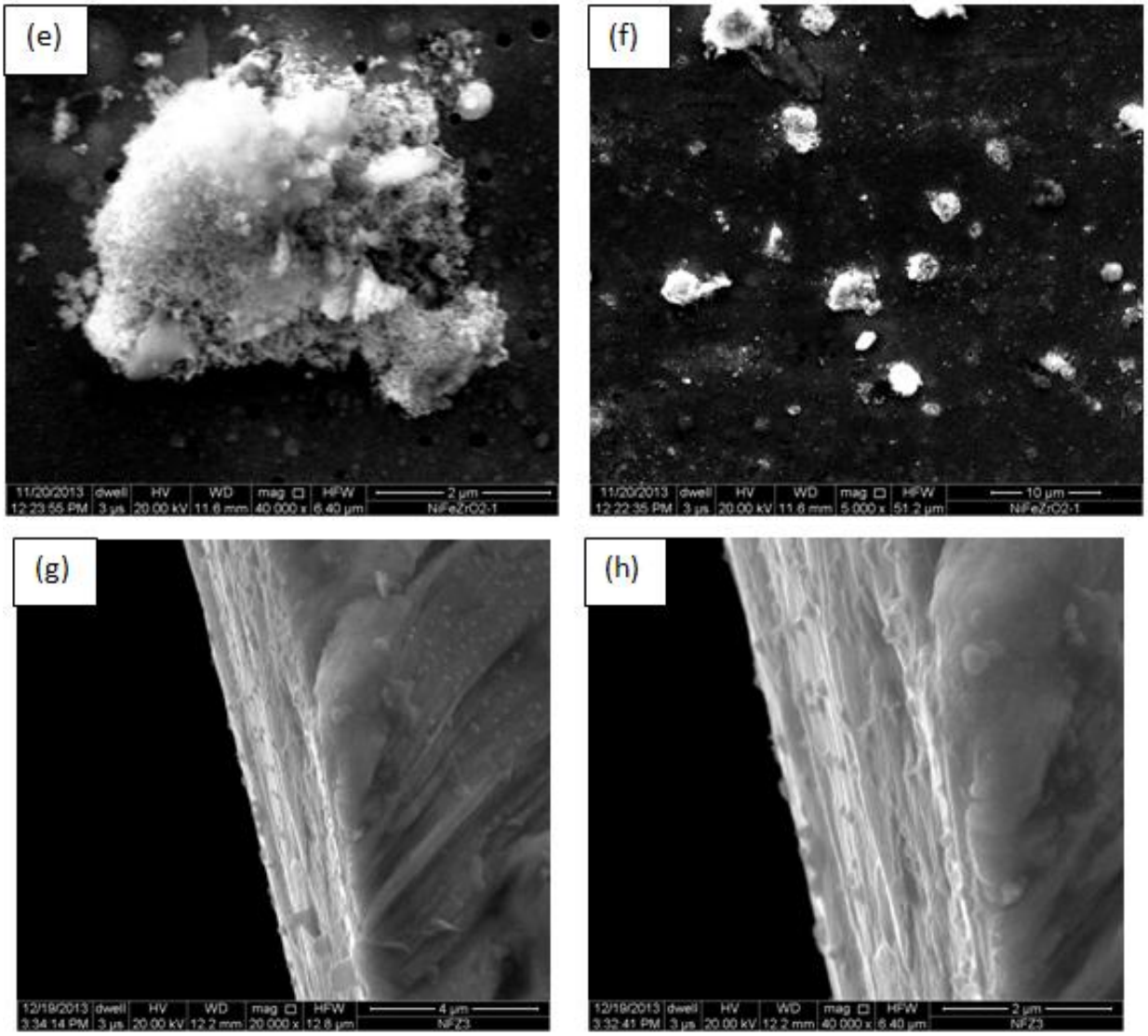

Figure 4. SEM micrograph of Ni-Fe/ZrO_2 nanocomposites at different current densities and magnifications. (a) 1.0 A/dm^2, (b) 3.0 A/dm^2, (c) & (d) 4.0 A/dm^2, (e) 1.0 A/dm^2, (f) 1.0 A/dm^2, (g) cross section at 1.0 A/dm^2, (h) cross section at 1.0 A/dm^2, (Conditions of the deposition: Nickel sulfamate 100 g/l, ferrous sulphate 4.0 g/l, boric acid 30 g/l, ZrO_2 particle 5.0 g/l, stirring rate 700 rpm, temperature 34±0.5°C).

It can be clearly identified from the figure that with increasing current density the size of the grains does not vary much and it is also further supported by XRD results. It can be examined from figure 4: (c) that ZrO_2 particles are uniformly distributed and monodispersed throughout the Ni-Fe matrix. Incorporation of ZrO_2 particles in the metal matrix results in fine grained granular structure of the deposits. Zirconia particles are observed to gather (figure 4: e, f) in small aggregates at lower current densities which is confirmed by EDAX analysis. At lower current density the rate of metal deposition is relatively low than the availability of ZrO_2 particles. Thus possibility of minor aggregation of particles can not be ignored. Composites prepared at relatively lower current densities (up to current density 3.0 A/dm^2) are found to be free from pores and cracks and have smooth and bright surfaces while at higher current densities they consisted of pores and cracks (figure 4: d).

In order to verify both the presence and the distribution of the ZrO_2 particles in the Ni-Fe alloy matrix, cross sectional examination of the coating was done by SEM which clearly reflects that ZrO_2 particles are uniformly embedded in the alloy matrix (figure 4: g & h).

3.4 Microstructural characterization through TEM

The microstructure and crystallographic structure of the nanocomposites were studied by Transmission Electron Microscope (TEM) and these are depicted in figure 5: (a) to (d). It is examined from the micrographs that dislocations and defects are not apparent in the microstructure (figure 5: a & b) and granular growth with distinct grain boundaries in the deposits is visible.

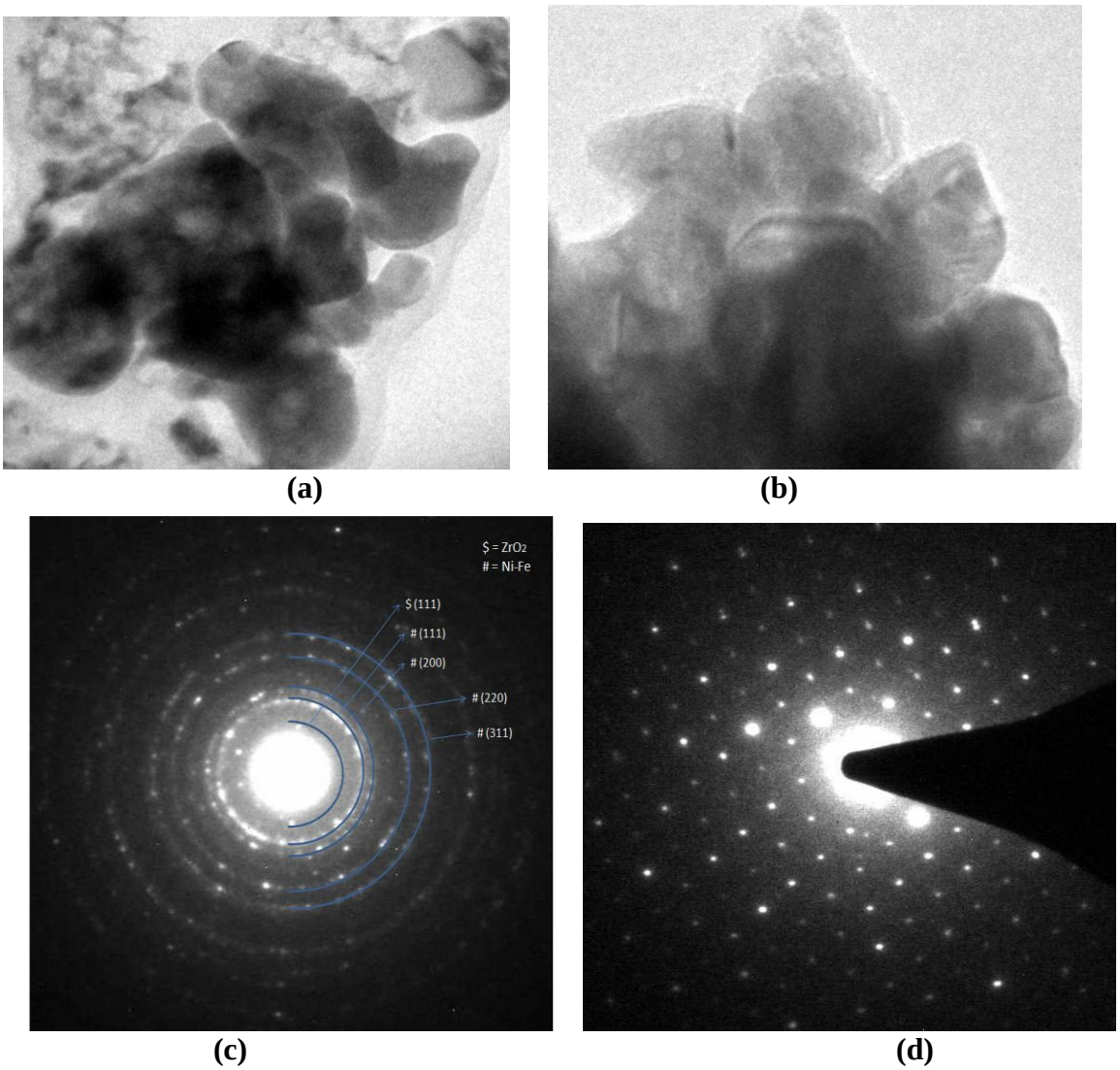

Figure 5. (a) & (b) TEM bright field image along with their corresponding selected area diffraction (SAD) pattern of Ni-Fe/ZrO_2 nanocomposite: (c) Polycrystalline material, (d) superlattice reflections [001] for an $L1_2$ ordered structure (Conditions of the deposition: Nickel sulfamate 100 g/l, ferrous sulphate 4.0 g/l, boric acid 30 g/l, ZrO_2 particle 5.0 g/l, stirring rate 700 rpm, temperature 34±0.5°C, current density 3.0 A/dm^2).

The grain mottled contrast indicating crystallite grain. The size of the grains is found in between 50 to 60 nm in the composite, throughout the sample. Electrodeposited Ni-Fe alloy of the corresponding composition has been reported[48] to show fcc structure with a larger probability of forming ordered Ni3Fe in nanocrystalline nickel iron alloys. The electron diffraction pattern (figure 5: c) indexed on the basis of face centered cubic lattice corresponding to Ni-Fe alloy solid solution together with monoclinic ZrO_2 particles. Presence of numerous spots on the ring diffraction pattern is considered to the characteristic of fine grained, polycrystalline randomly oriented material. As such SAD pattern does not clearly indicate texturing in the deposits. The values of lattice parameter obtained from the electron diffraction pattern is found to be 3.53Å (±0.02Å) which is slightly higher than the standard value of pure nickel and closer to the Ni_3Fe (3.55Å). These values shows the formation of ordered intermetallic Ni_3Fe, similer to those reported earlier[26,27]. Figure 5: d is selected area diffraction (SAD) pattern corresponding to single crystal, was indexed which revealed Ni_3Fe ordered phase and a comparison showed that the diffraction corresponded along [011] zone axis. In such ordered phase with an $L1_2$ ordered configuration, the Ni atoms occupy the face-centered site, while the Fe atom occupies the corner site in one unit cell. It is reported earlier that ordered phase shows superlattice reflections for an $L1_2$ ordered structure, such as [011] $L1_2$[48]. Presence of superlattice reflection evidences the absence of defects and dislocations in the matrix.

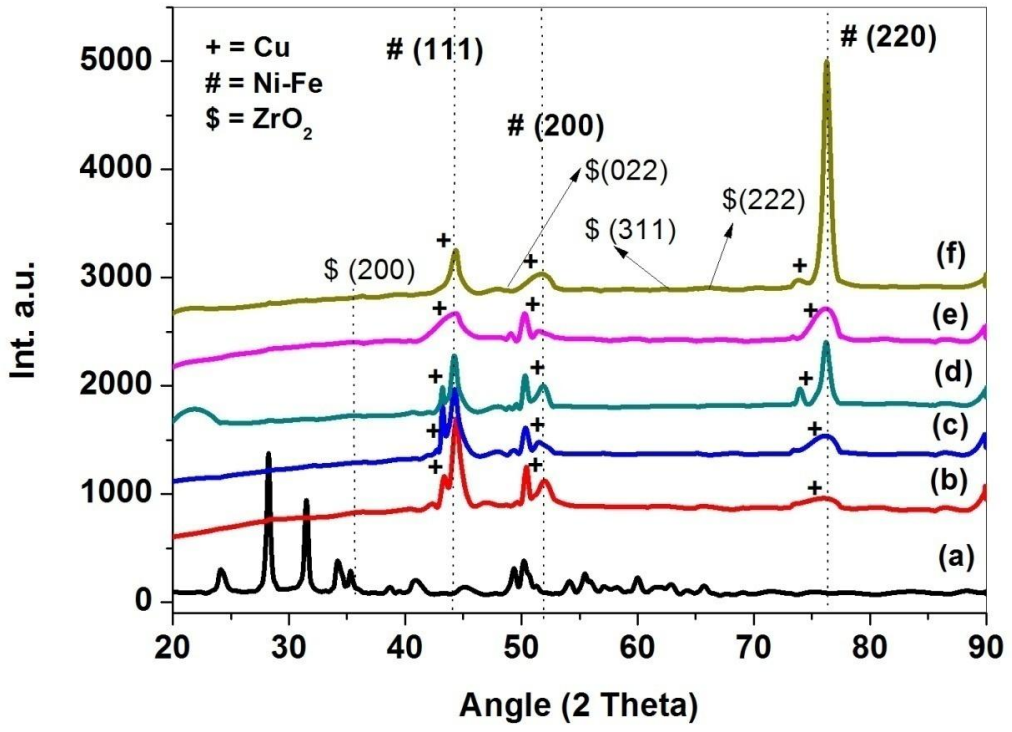

Figure 6. XRD pattern of ZrO_2 nanopowder (a) and as deposited Ni-Fe/ZrO_2 nanocomposites prepared at current density (b) 1.0 A/dm^2 (c) 2.0 A/dm^2 (d) 3.0 A/dm^2 (e) 4.0 A/dm^2 (f) 5.0 A/dm^2. (Conditions of the deposition: Nickel sulfamate 100 g/l, ferrous sulphate 4.0 g/l, boric acid 30 g/l, ZrO_2 particle 5.0 g/l, stirring rate 700 rpm, and temperature 34±0.5°C).

3.5. XRD Study

The X-ray diffraction spectra of as electrodeposited Ni-Fe/ZrO_2 nanocomposites at different current densities are shown in figure 6. The X-ray diffraction spectra shows typical peaks corresponding to (111), (200) and (220) crystallographic planes with crystalline fcc structure. At lower current densities, the coatings are found to exhibit a predominant (111) reflection while nanocomposites electrodeposited at higher current densities show preferred growth along (220) crystallographic plane. The relative texture coefficient (RTC) calculation reveal that with increasing current density RTC along (111) crystallographic plane decreases and along (220) crystallographic plane it increases (Table 2). At high current density (5.0 A/dm^2) RTC along (220) plane approaches towards unity indicating maximum growth along that plane. There are two probable aspects which might be considered to influence the texture of the deposit with change in the current density. The first one may be due to the particle incorporation which does not seem to be much effective to bring change in the texture because change in texture is not according to the content of the particles incorporated in the nanocomposite.

The other possibility of change in texture is due to the hydrogen evolution, and its inclusion in the deposit. According to Reddy[49], texture changes are induced by surface hydrogen atoms and deposits having different textures should have different hydrogen contents and roughly free energy of hydrogen adsorption may be less negative with decreasing inter site spacing. The planes with less adsorbed atomic hydrogen coverage will show preferential growth. If we examine our results in the light of this proposition it is expected that with increasing current density more hydrogen is likely to be evolved and it can be concluded that with increasing hydrogen evolution the surface of the cathode modifies and alters the deposition process favoring the preferred orientation along (220) plane.

Table 2. Relative texture coefficients of the different (hkl) planes.

C.D. (A/dm^2)	Crystallite size (nm)	Strain	Relative Texture coefficient		
			(111)	(200)	(220)
1.	10.94	0.0076	0.44	0.31	0.25
2.	10.10	0.0117	0.38	0.14	0.48
3.	13.33	0.0036	0.14	0.12	0.74
4.	10.60	0.0103	0.14	0.08	0.78
5.	14.18	0.0035	0.04	0.03	0.93

Similar results were found by other investigators [37,50]. The intensities of ZrO_2 particle peaks are feeble nevertheless it can be identified at angles 17.648 (200), 24.75° (022), 31.40 (311), 32.835 (222) in each XRD patterns which confirms the incorporation of ZrO_2 particles in the alloy matrix. The deposits showed fcc lattice with lattice constant 3.51 Å to 3.55 Å which is slightly higher than the standard value of pure nickel and closer to intermetallic Ni_3Fe, indicating the formation of more ordered Ni_3Fe[26]. The crystallite size calculations of all the deposits from optimum bath yielded that there is not much variation and all have crystallite size ≈11 nm. Almost negligible strain is noticed in

the coating (table 2). This is probably due to the grain refinement of the alloy matrix by ZrO_2 particles in the composite coating resulting in smaller crystallite size. The crystallite size of Ni-Fe alloys is also dependent on the iron content of the deposit and it is reported[26] that grain size remains approximately constant (≈11 nm) for electrodeposited Ni-Fe fcc alloys with the iron content in the range 21% to 51%.

3.6 Thermal analysis

Ni-Fe/ZrO_2 nanocomposites were annealed at 800°C for 1 hour and resulting changes in crystalline structure, crystalline structure, and phase transitions are examined. The XRD peaks of the deposits become remarkably sharp in comparison to the as deposited after the heat treatment which is due to the recrystallization and grain growth (figure 7).

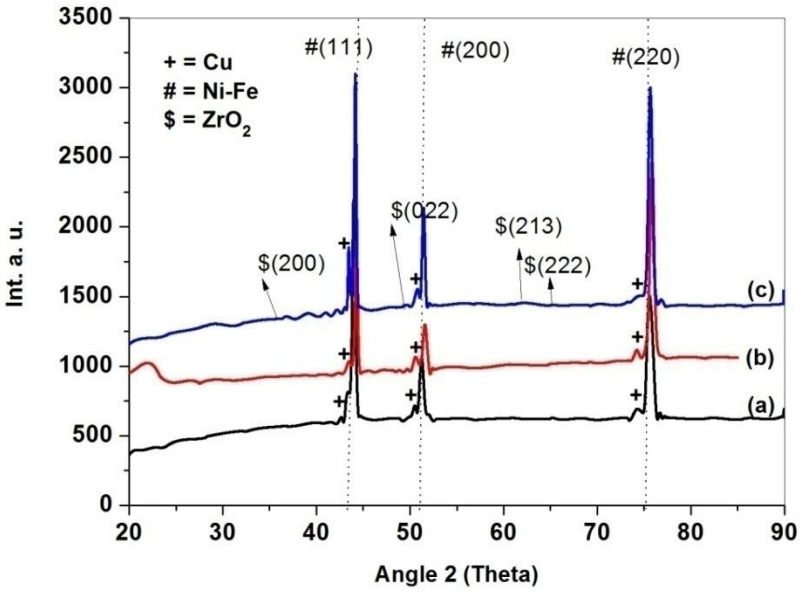

Figure 7. XRD pattern of annealed Ni-Fe/ZrO_2 nanocomposites prepared at current density (a) 1.0 A/dm^2 (b) 3.0 A/dm^2 (c) 5.0 A/dm^2. (Conditions of the deposition: Nickel sulfamate 100 g/l, ferrous sulphate 4.0 g/l, boric acid 30 g/l, ZrO_2 particle 5.0 g/l, stirring rate 700 rpm, and temperature 34±0.5°C).

It is evident from the figure that after annealing, the growth of the deposit along (111) plane increases as compared to the as deposited nanocomposites. The observed growth along (111) plane is considered due to the fact that the plane (111) has lowest surface energy, therefore the recrystsllization and grain growth are obtained along that plane[49]. An increase in the lattice constant is also observed as a result of annealing. Lattice constant for as deposited Ni-Fe/ZrO_2 nanocomposites is found to be 3.518 Å to 3.551 Å while the value for the annealed deposits ranged between 3.544 Å to 3.567 Å. DSC measurements indicate that formation of an intermetallic phase (Ni_3Fe) in the composite can not be ignored. A broad exothermic peak around 630°C is observed in DSC curve which suggests the formation of an ordered phase (figure 8). Evaluation of lattice parameters of the annealed deposits

gives closer values to the lattice constant of Ni_3Fe (3.555 Å) which supports the DSC measurements. It is also noticeable (table 3) that the crystallite size increases while strain decreases upon annealing of the deposits in comparison with as deposited composites. This is considered due to recrystallization and consequently grain growth due to heat treatment.

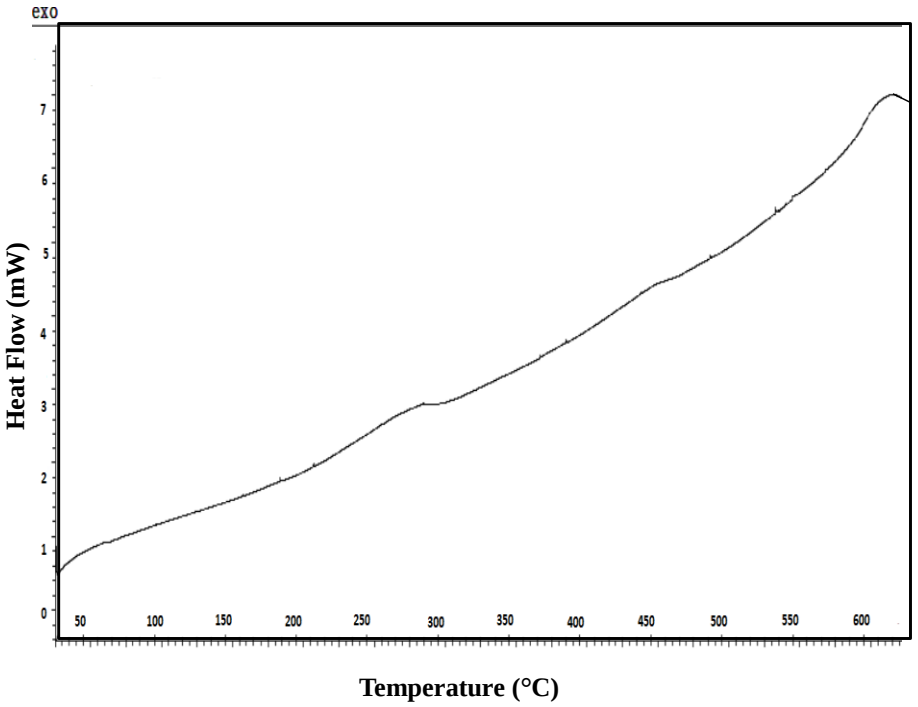

Figure 8. DSC trace of Ni-Fe/ZrO_2 nanocomposite. (Conditions of the deposition: Nickel sulfamate 100 g/l, ferrous sulphate 4.0 g/l, boric acid 30 g/l, ZrO_2 particle 5.0 g/l, stirring rate 700 rpm, and temperature 34±0.5°C, C.D. 3.0 A/dm^2).

Table 3. Variation in crystallite size and strain of as deposited coatings after annealing at 800°C for 1 hour.

C.D. (A/dm^2)	Crystallite Size (nm)		Strain	
	As deposited	Annealed	As deposited	Annealed
1.0	10.94	23.82	0.0076	0.0054
3.0	13.33	17.95	0.0036	0.0027
5.0	14.18	33.06	0.0035	0.0023

3.7 Microhardness

The influence of current density on the microhardness of the as deposited nanocomposites and after annealing at 800°C for 1 hour is illustrated in table 4. The microhardness of the as deposited Ni-

Fe alloy increases slightly at lower current densities and remains approximately constant at higher current densities (3.0 to 5.0 A/dm^2). Ni-Fe/ZrO_2 nanocomposites have shown improved microhardness as compared to Ni-Fe alloy. An improved microhardness of the Ni-Fe/ZrO_2 nanocomposite as compared to Ni-Fe alloy coating is due to the presence of the dispersed ZrO_2 particles. The microhardness value of the nanocomposite coatings ranged between 590 HV and 842 HV. Table 4 shows an initial increase in the microhardness up to current density 4.0 A/dm^2 and thereafter it decreases. The variation in microhardness with varying ZrO_2 content shows a good correspondence, however, does not match exactly with current density. The grain refinement of Ni-Fe matrix by ZrO_2 particles in the nanocomposite coating results in a higher strengthening effect. Increasing dispersion of ZrO_2 particles in the alloy matrix should result in a high strengthening effect by the Orowan mechanism [51]. Maximum hardness is observed at current density 4.0 A/dm^2 having a lower particle incorporation than that of current density 2.0 A/dm^2. Hardness is also a function of the iron content in the Ni-Fe alloy, and it increases with decreasing iron content and maximum hardness at about 21wt% iron is reported due to formation of ordered Ni_3Fe. Such increase in microhardness may be associated with the ordering of the structure. With further decrease in iron content microhardness decreases [26, 27]. However, coatings show improved hardness than alloy due to incorporation of ZrO_2 particles. This is probably due to the fact that hardness does not depends only on the particle content of the deposit but more importantly on the size and the distribution of the particles in the metal matrix[51] and also on composition of alloy matrix. The results are similar to those reported earlier [1, 51] where microhardness of the deposits having lower particle incorporation having a higher microhardness value. All the deposits are having approximately similar grain size (≈11 nm) thus microhardness of the deposits does not show much dependence on the grain size in this range [26].

Table 4. Effect of current density on microhardness value of Ni–Fe/ZrO_2 nanocomposite. (Conditions of the deposition: Nickel sulfamate 100 g/l, ferrous sulphate 4.0 g/l, boric acid 30 g/l, ZrO_2 particle 5.0 g/l, stirring rate 700 rpm, and temperature 34±0.5°C).

C.D. (A/dm^2)	As deposited alloy (HV)	As deposited nanocomposite (HV)	Annealed nanocomposite (HV)
1.0	570	590	150
2.0	590	620	160
3.0	707	737	171
4.0	730	842	202
5.0	750	781	238

The variation in microhardness of heat treated Ni-Fe/ZrO_2 coatings has been shown in table 4. The deposits annealed at 800°C showed a marked decline in microhardness with respect to as deposited one e.g. 842 HV reduced to 202 HV. Similar dependence of hardness with respect to annealing temperature was observed by other workers[1,4]. It seems that initially there is relief of the internal stress existed in the deposit as a result of cold working. Considerable decrease in

microhardness of the annealed deposits is observed which is due to the fact that there grain growth occurs at higher temperature because of more mobility of ions which favors the formation of larger grains resulting in a considerable decrease in the microhardness, which is also supported by XRD results.

4. CONCLUSION

In the present investigation it was observed that the electrodeposition of Ni-Fe/ZrO_2 nanocomposites was affected by several factors including current density, temperature and agitation etc. Smooth, bright and adherent deposits were obtained with a maximum of 36 weight% ZrO_2 incorporation in the alloy deposits. In comparison with parent alloy, nanocomposite deposits possessed superior hardness. The microhardness value of the nanocomposite coatings ranged between 590 HV and 842 HV while that of Ni-Fe alloy was ranged between 570 and 750 HV. Results of the investigation indicated that microhardness of the nanocomposites is not only dependent on the content of incorporated particles but also significantly upon the microstructure, nature, extent of reinforcement and composition of alloy matrix. TEM studies revealed that the size of the grains ranged between 50 to 60 nm with distinct grain boundaries. The electron diffraction pattern showed fine grained polycrystalline randomly oriented and single crystalline nature. The deposits owned very low strain and possessed crystallite size ≈11 nm. Lattice parameters of the deposits were found slightly higher than the standard lattice parameter of nickel and closer to the intermetallic Ni_3Fe ordered phase. At higher current density there was some indication of texture formation along (220) crystallographic plane.

ACKNOWLEDGEMENT
Financial assistance provided by the Council of Scientific and Industrial Research, CSIR, New Delhi, India, is gratefully acknowledged. TEM facility provided by Prof. O.N. Shrivastava department of Physics BHU and microhardness testing availed from department of Metallurgy I.I.T. BHU are also thankfully acknowledged.

References

1. D. K. Singh and V. B. Singh, *Mater. Sci. Engg. A*, 532, (2012) 493.
2. H. Gul, F. Kilic, S. Aslan, A. Alp and H. Akbulut, *Wear*, 267, (2009) 976.
3. R. Arghavanian and N. P. Ahmadi, *J. Solid State Electrochem.,* 15, 2199 (2011).
4. M. Srivastava, A. Srinivasan and V. K. W. Grips, Am. *J. Mater. Sci.,* 1(2), 113 (2011).
5. D. Shui, Z. Kaifeng and W. Changli, *J. Wuhan Univ. Technol.,* 22(3), 462 (2007).
6. X. S. Liang, J. H. Ouyang, Y. F. Li and Y. M. Wang, *Appl. Surf. Sci.,* 255, 4316 (2009).
7. I. Garcia, A. Conde, G. Langelaan, J. Fransaer and J. P. Celis, *Corros. Sci.*, 45, 1173 (2003).
8. Y. Zhou, H. Zhang and B. Qian, *Appl. Surf. Sci,.* 253, (2007) 8335.
9. D. K. Singh and V. B. Singh, *J. Electrochem. Soc.,* 158 (2), (2011) D114.
10. M. K. Tripathi, D. K. Singh and V. B. Singh, *Int. J. Electrochem. Sci.,* 8, (2013) 3454.
11. F.H. Stott and D.J. Ashby, *Corr. Sci.*, 18(3), (1978) 183.
12. B. S. B. Reddy, K. Das, A. Kumar Datta and S. Das, *Nanotechnology,* 19, (2008) 115603.
13. S. R. Bakshi, D. Lahiri and A. Agarwal, *Int. Mater. Rev.,* 55 (1), (2010) 41.

14. J. Lu, J. B. Zang, S. X. Shan, H. Huang and Y. H. Wang, *Nano Lett.*, 8 (11), (2008) 4070.
15. A. M. Rodriguez, A. B. Leon, A. D. Rodriguez, S. L. Esteban, J. S. Moya and M. J. Melendo, *J. Eur. Cerm. Soc.*, 23, (2003) 2849.
16. P. A. Gay, P. Bercot and J. Pagetti, *Surf. Coat. Technol.*, 140, (2001) 147.
17. L. Benea, P. Ponthiaux and F. Wenger, *Surf. Coat. Technol.*, 205, (2011) 5379.
18. S. Surviliene, A. L. Oleksiak and A. Cesuniene, *Corros. Sci.*, 50, (2008) 338.
19. B. Szczygieł and A. Turkiewicz, *Appl. Surf. Sci.*, 255, (2009) 8414.
20. F. Hou, W. Wang and H. Guo, *Appl. Surf. Sci.*, 252, (2006) 3812.
21. F. Fernandes, A. Ramalho , A. Loureiro, J. M. Guilemany, M. Torrell and A. Cavaleiro, *Wear*, 303, (2013) 591.
22. K. Vathsala and T. V. Venkatesha, *Appl. Surf. Sci.*, 257, (2011) 8929.
23. Y. Yao, M. Zhao, C. Zhao and H. Zhang, *Electrochim. Acta*, 117, (2014) 453.
24. S. V. Eremeev, S. Schmauder, S. Hocker and S. E. Kulkova, *Surf. Sci.*, 603, (2009) 2218.
25. Y. V. Timoshkov, I. S. Molchan, S. V. Labunov, V. I. Kurmashev, T. M. Gubarevich, J. Fransaer and J. P. Celis, Surface Modification Technologies, vol. XI, p. 991, Institute of Materials, London (1998).
26. H. Li and F. Ebrahimi, *Mater. Sci. Eng. A*, 347, (2003) 93.
27. H.Q. Li and F. Ebrahimi, *Acta Mater.*, 51,(2003) 3905.
28. X. Y. Qin, R. Cao and J. Zhang, *Compos. Sci. Technol.*, 67, (2007) 1530.
29. S. V. Eremeev, S. Schmauder, S. Hocker and S. E. Kulkova, *Surf. Sci.*, 603, (2009) 2218.
30. S. Biallozor, and M. Lieder, *Surf. Technol.*, 21, (1984) 1.
31. J. H. Kim, T.H. Yim and J. H. Lee, *Curr. Appl. Phys.*, 13 (2), (2013) S108.
32. A. Brenner, Electrodeposition of alloys: Principals and practice, Vol. II, p. 267, Academic Press, New York & London (1963).
33. T. Krause, L. Arulnayagam, and M. Pritzker *J. Electrochem. Soc.* 144(3), (1997) 960.
34. D. Singh and V. B. Singh, *Ind. J. Technol.*, 158 (2), (1975) D114.
35. H. Li, F. Czerwinski and J. A. Szpunar, *Nanostr. Mater.*, 9, (1997) 673.
36. T. Takei, *J. Appl. Electrochem.*, 9, (1979) 587.
37. V. B. Singh and R. S. Sarabi, *Mater. Chem. Phys.*, 34, (1993) 238.
38. A. A. Sarabi and V. B. Singh, *T. Jpn. I. Met.*, 28, (1987) 916.
39. P. Scherrer , *Gott. Nachr.*, 2, *(*1918) 98.
40. T. H. D. Keijser, J. I. Langford, E. J. Mittemeijer and A. B. P. Vogels, *J. Appl. Cryst.*, 15, (1982) 308.
41. E. J. Mendham, R.C. Denney, J.D. Barnes and M. Thomas, Vogel's Textbook of Quantitative Chemical Analysis 6th Edn., p. 394, Pearson Education Asia, (2003).
42. H.E. Boyer, (Ed) Hardness Testing, ASM International, Metals Park, OH (1987).
43. L. R. Nylandaenrd, S. F. Pavkovic, *Inorganic Chem.*, Vol. 9, No. 8, (1959) 1970.
44. I. Labadi, G. Liptay, A. Horvath, L. Korecz, S. Papp and K. Burger, *J. Thermal Analysis*, 32, (1987) 1575.
45. R. Gomer and G. N. Tyson, *J. Am. Chem. Soc.*, 66 (1944) 1331.
46. M. R. Vaezi, S. K. Sadrnezhaad and L. Nikzad, *Colloid. Surface. A*, 315, (2008) 176.
47. Y. Yao, S. Yao, L. Zhang, H. Wang, *Mater. Lett.*, 61, (2007) 67.
48. X. Zhong, J. Zhu and A. Zhang, *Intermetallics*, 15, (2007) 495.
49. A. K. N. Reddy, *J. Electroanal. Chem.*, 6, (1963) 141.
50. V. B. Singh and R. S. Sarabi, *Mater. Chem. Phys.*, 39, (1994) 124.
51. W. Wang, F. Y. Hou, H. Wang and H. T. Guo, *Scripta Mater.*, 53, (2005) 613.